Ab initio lattice dynamics and charge fluctuations in alkaline-earth oxides

O. Schütt, P. Pavone, W. Windl, K. Karch, and D. Strauch
Institut für Theoretische Physik, Universität Regensburg, D-93040 Regensburg, Germany
(Received 15 October 1993; revised manuscript received 26 April 1994)

We present an *ab initio* calculation of lattice-dynamical properties of the alkaline-earth oxides MgO, CaO, and SrO in the rocksalt structure. We employ the density-functional perturbation theory within the local-density approximation. We show phonon dispersion curves along several symmetry directions in the Brillouin zone. The calculated frequencies agree well with the available experimental data. The investigation of the phonon-induced charge-density fluctuations of MgO and CaO at the L point of the Brillouin zone partially supports the breathing-shell model of lattice dynamics and rules out the charge-transfer model for this class of materials. Moreover, our calculations show that the breathinglike charge-density response is more pronounced for oxygen than for the cations in these compounds.

I. INTRODUCTION

Looking back at a long history of scientific interest, the presence of oxygen in different compounds has given rise to a manifold of speculations. The peculiarity of oxygen to react significantly to the chemical environment in the crystal manifests itself for example in the polarizability of the oxygen.[1–4] In the alkaline-earth oxides, all crystallizing in the rocksalt structure, the polarizability $\alpha(O^{2-})$ of the oxygen ion is proportional to the unit-cell volume V, and in tetrahedrally bonded oxides one finds $\alpha(O^{2-}) \propto V^2$, whereas in spinels or ferroelectric oxides the anisotropic configuration of the oxygen causes a proportionality of the polarizability to V^β with $3 \leq \beta \leq 4$. Also in ferroelectrics the oxygen seems to play the dominating role: 99% of the known ferroelectrics are chalcogenides and especially 97% of them are oxides.[5]

Big differences also occur in the ground-state charge densities. Simple oxides like MgO, CaO, or SrO are predominantly ionic insulators with spherically symmetric charge densities about each ion.[6–8] Transition-metal oxides like RuO_2 or TiO_2 crystallize in the rutile structure and exhibit covalent bonding behavior.[9–11] Ionic *and* covalent bonds of the oxygen ion can be found in one and the same crystal, for example, in the oxysalt system magnesite ($MgCO_3$) which contains a covalently bonded molecular unit (the $CO_3{}^{2-}$ anion), with mainly ionic interaction with the metal cation.[12] However, the interaction of the magnesium ion with the oxygen in magnesite in comparison with MgO is shifted towards covalency.

Our purpose is to give a detailed description of the lattice-dynamical properties of the simple alkaline-earth oxides MgO, CaO, and SrO using the method of the density-functional perturbation theory (DFPT).[13–16] This theory allows the self-consistent calculation of the linear response of a system to an external perturbation, combining the advantages of the frozen-phonon method[17–19] and of the dielectric theory.[20–22] For the calculation of the density response only unperturbed quantities are needed. There is no restriction to high-symmetry points as in a frozen-phonon calculation; in principle, perturbations of arbitrary wavelength can be calculated.

For a practical implementation of the DFPT we employ the plane-wave pseudopotential method (PWPM). For a long time a description in terms of the PWPM has been believed to be unfeasible for compounds involving first-row elements such as carbon or oxygen. However, due to the recent efforts in developing "soft" pseudopotentials[23] this kind of calculation seems to be within modern supercomputer possibilities.

In this work, the phonon dispersion curves along several high-symmetry directions in the Brillouin zone are presented. As a by-product we obtain various ground-state properties: the lattice constant, the bulk modulus, the effective charges, and the high-frequency dielectric constant. The theoretical results for all these quantities are in good agreement with the available experimental values.

Additionally, we present phonon-induced charge-density changes for MgO and CaO. These results allow the investigation of the above-mentioned sensitivity of the oxygen ion to phonon-induced charge fluctuations, with implications for phenomenological lattice-dynamical models.

The paper is organized as follows: Section II gives a short outline of the theory, concentrating on linear response and lattice dynamics. In Sec. III we present the results for pseudopotentials, ground-state properties, phonons, and charge fluctuations. Finally, some conclusions are drawn in Sec. IV.

II. THEORETICAL FRAMEWORK

A. Unperturbed quantities and pseudopotentials

The structural and electronic properties of the alkaline-earth oxides are calculated in the framework of density-functional theory, using the local-density approximation (LDA) for the exchange-correlation interaction. We describe the interaction of the electrons with the ion cores by norm-conserving pseudopotentials generated following a scheme proposed by Troullier and Martins.[23] These "soft" and efficient pseudopotentials guarantee fast convergence for expansions in terms of plane waves, even for compounds containing first-row elements like carbon or

oxygen. The main difficulties created by such elements can be related to the presence of $2p$ wave functions among the valence states. In fact, first-row elements have no p levels in the core; then the $2p$ states do not need to be pushed away from the nucleus due to the orthogonality with equivalent (i.e., with the same angular momentum) core states. Thus, these $2p$ valence states are strongly localized.

B. Linear response and lattice dynamics

The calculation of phonon frequencies for a given $\mathbf{q}$ vector requires the solution of the eigenvalue problem

$$\sum_{\kappa'} \mathbf{D}(\kappa\kappa'|\mathbf{q}) \cdot \mathbf{e}^j(\kappa'|\mathbf{q}) = \omega_j^2(\mathbf{q})\, \mathbf{e}^j(\kappa|\mathbf{q}) \tag{1}$$

for the dynamical matrix $\mathbf{D}$. Here κ and κ' label the sublattices, ranging from 1 to N. The eigenvectors $\mathbf{e}^j(\kappa|\mathbf{q})$ and eigenfrequencies $\omega_j^2(\mathbf{q})$ of the dynamical matrix are labeled by the $3N$ branch indices j. The dynamical matrix (in the harmonic approximation) is the Fourier transform of the force-constant matrix $\mathbf{\Phi}$,

$$D_{\alpha\beta}(\kappa\kappa'|\mathbf{q}) = \frac{1}{\sqrt{M_\kappa}} \sum_l \Phi_{\alpha\beta}\binom{0\ l}{\kappa\ \kappa'} \exp[i\mathbf{q}\cdot\mathbf{R}(l)] \frac{1}{\sqrt{M_{\kappa'}}}, \tag{2}$$

where M_κ denotes the mass of the κth atom, l numbers the elementary cells, and $\mathbf{R}(l)$ is the corresponding Bravais lattice vector. The force constants are the second derivatives of the total energy E of the crystal with respect to the atomic displacements $\mathbf{u}\binom{l}{\kappa}$. The force-constant matrix can be divided into an electronic and an ionic contribution,

$$\mathbf{\Phi}\binom{l\ l'}{\kappa\ \kappa'} = \mathbf{\Phi}^{\mathrm{el}}\binom{l\ l'}{\kappa\ \kappa'} + \mathbf{\Phi}^{\mathrm{ion}}\binom{l\ l'}{\kappa\ \kappa'}. \tag{3}$$

The ionic part can be calculated classically using an Ewald summation technique.[15]

For the electronic part one obtains, with the help of the Hellmann-Feynman theorem,[24]

$$\Phi^{\mathrm{el}}_{\alpha\beta}\binom{l\ l'}{\kappa\ \kappa'} = \int \left\{ \frac{\partial\rho(\mathbf{r})}{\partial u_\alpha\binom{l}{\kappa}} \frac{\partial V_{\mathrm{ion}}(\mathbf{r})}{\partial u_\beta\binom{l'}{\kappa'}} + \rho(\mathbf{r}) \frac{\partial^2 V_{\mathrm{ion}}(\mathbf{r})}{\partial u_\alpha\binom{l}{\kappa} \partial u_\beta\binom{l'}{\kappa'}} \right\} d^3r. \tag{4}$$

V_{ion} denotes the bare ionic (pseudo)potential, ρ the charge density of the unperturbed system, and $\partial\rho/\partial u_\alpha\binom{l}{\kappa}$ the response of the system to a displacement $u_\alpha\binom{l}{\kappa}$ of the ion $\binom{l}{\kappa}$ in the α direction. All the derivatives are calculated at zero displacements. Instead of solving this problem in direct space and then taking the Fourier transform one can directly calculate the dynamical matrix via Eq. (2) by considering a phonon with displacements of the form

$$\mathbf{u}\binom{l}{\kappa} = \mathbf{u}(\kappa|\mathbf{q}) \exp[i\mathbf{q}\cdot\mathbf{R}\binom{l}{\kappa}]. \tag{5}$$

Then, one immediately obtains for a crystal with N_c unit cells

$$\sqrt{M_\kappa}\, D_{\alpha\beta}(\kappa\kappa'|\mathbf{q})\, \sqrt{M_{\kappa'}} = \frac{1}{N_c} \int \left(\frac{\partial\rho(\mathbf{r})}{\partial u_\alpha(\kappa|\mathbf{q})} \right)^* \frac{\partial V_{\mathrm{ion}}(\mathbf{r})}{\partial u_\beta(\kappa'|\mathbf{q})}\, d^3r + \delta_{\kappa\kappa'} \frac{1}{N_c} \int \rho(\mathbf{r}) \frac{\partial^2 V_{\mathrm{ion}}(\mathbf{r})}{\partial u_\alpha(\kappa|\mathbf{q}=0) \partial u_\beta(\kappa|\mathbf{q}=0)}\, d^3r. \tag{6}$$

The knowledge of the response of the system to a lattice distortion yields the harmonic force constants or equivalently the dynamical matrix. The calculation of the response $\partial\rho/\partial\mathbf{u}$ of the system is performed self-consistently within the framework of DFPT. A complete and detailed outline of the theory is given in Refs. 15 and 16.

Furthermore, the difference $\Delta\rho^j_{\mathbf{q}}(\mathbf{r})$ between the charge densities $\rho^j_{\mathbf{q}}(\mathbf{r})$ of the displaced and $\rho(\mathbf{r})$ of the undisplaced system, linear in the eigenvectors of the dynamical matrix, is

$$\Delta\rho^j_{\mathbf{q}}(\mathbf{r}) = \rho^j_{\mathbf{q}}(\mathbf{r}) - \rho(\mathbf{r}) \cong \sum_{\kappa\alpha} \frac{\partial\rho(\mathbf{r})}{\partial u_\alpha(\kappa|\mathbf{q})}\, w^j_\alpha(\kappa|\mathbf{q}), \tag{7}$$

where the $\mathbf{w}^j(\kappa|\mathbf{q})$ are the *eigendisplacements* of the dynamical matrix, i.e., the eigenvectors $\mathbf{e}^j(\kappa|\mathbf{q})$, first divided by the square root of the mass $\sqrt{M_\kappa}$, and *then* normalized to 1. Obviously, due to this normalization the charge variations in Eq. (7) are "unphysically" too large. However, they can be considered a magnification of what one obtains for actual phonon displacements.

C. Polar compounds

In polar materials, the longitudinal optic phonons in the limit $\mathbf{q} \to 0$ give rise to a macroscopic electric field caused by the long-range part of Coulomb forces. This leads to a nonanalytic behavior of the force constants and correspondingly of the dynamical matrix,

$$\mathbf{D}(\kappa\kappa'|\mathbf{q}\to 0) = \mathbf{D}^{\mathrm{an}}(\kappa\kappa'|\mathbf{q}\to 0) + \mathbf{D}^{\mathrm{na}}(\kappa\kappa'|\mathbf{q}\to 0). \tag{8}$$

The nonanalytic part can generally be written as

$$D^{\mathrm{na}}_{\alpha\beta}(\kappa\kappa'|\mathbf{q}\to 0) = \frac{4\pi e^2}{V} \frac{(\mathbf{q}\cdot\mathbf{Z}^*_\kappa)_\alpha\, (\mathbf{q}\cdot\mathbf{Z}^*_{\kappa'})_\beta}{\mathbf{q}\cdot\boldsymbol{\epsilon}_\infty\cdot\mathbf{q}}. \tag{9}$$

Thus, the complete information for describing the nonanalytic part is contained in the knowledge of the tensor $\mathbf{Z}^*_\kappa$ of the Born effective charges and the tensor $\boldsymbol{\epsilon}_\infty$ of the macroscopic high-frequency dielectric constant. These quantities, too, are calculated self-consistently in the framework of DFPT.[15] The analytic part of the dynamical matrix is calculated in the conventional way, i.e., neglecting any macroscopic polarization.

D. Computational details

Due to the use of "soft" norm-conserving pseudopotentials all quantities can be expanded in terms of a limited number of plane waves whose kinetic energy lies below a relatively small cutoff energy. The calculations for MgO, CaO, and SrO have been performed with a kinetic-energy cutoff of 65, 55, and 60 Ry, respectively, corresponding to 1592, 1780, and 2436 plane waves, respectively. In fact, convergence has been achieved in the case of MgO with 55 Ry.

We have used the parametrization of Perdew and Zunger[25] for the exchange-correlation energy in the LDA. The integrals in reciprocal space have been replaced by summations over ten special points[26] in the irreducible wedge of the Brillouin zone. Further technical details are identical with those of Ref. 15.

III. RESULTS

A. Norm-conserving pseudopotentials

The norm-conserving pseudopotentials for the four elements Mg, Ca, Sr, and oxygen exhibited their individual peculiarities during their construction. In view of the electronic structure [noble gas]ns^2 of the alkaline-earth metals the first choice would be to take only the two s electrons as valence electrons. However, inspection of the atomic energy-level diagram of Fig. 1 shows that for Ca (Sr) in the solid a strong hybridization of the $3p^6$ ($4p^6$) states with the oxygen $2s^2$ states can be expected. In the case of Mg it is sufficient to deal only with the $3s^2$ states as valence states due to the fact that the $2p^6$ energy is sufficiently far away from the valence-state energies of the oxygen.

The reference configurations we have chosen for the four elements are given in Table I. In order to improve the transferability of the pseudopotentials of the alkaline-earth metals we have included contributions also from excited states. These latter have been calculated with an ionized reference configuration.

In Table I we also list the chosen cutoff radii and the positions of the (all-electron) wave function maxima. We have found that the structural, electronic, and dynamic properties of the three oxides are essentially independent of the choice of the cutoff radii of the oxygen ion, but that they react sensitively to changes of the cutoff radii of the cations.

TABLE I. The coordinate of the maximum of the wave function, cutoff radius r_c, and reference configuration for each of the single elements.

	r_{max} (a.u.)	r_c (a.u.)	Reference configuration
Magnesium			
$l=0$	2.52	3.40	$3s^2$
$l=1$	3.10	3.00	$3s^{1.25}\ 3p^{0.25}$
Calcium			
$l=0$	3.30	3.35	$3p^6\ 4s^2$
$l=1$	1.05	2.00	$3p^6\ 4s^2$
$l=2$	1.30	2.50	$3p^6\ 4s^{1.25}\ 3d^{0.25}$
Strontium			
$l=0$	3.68	4.50	$4p^6\ 5s^2$
$l=1$	1.33	1.70	$4p^6\ 5s^2$
$l=2$	2.06	3.00	$4p^6\ 5s^{1.25}\ 4d^{0.25}$
Oxygen			
$l=0$	0.87	1.60	$2s^2\ 2p^4$
$l=1$	0.81	1.60	$2s^2\ 2p^4$

The Sr pseudopotential causes additional problems originating from the overlap of the charge density of the filled $3d^{10}$ shell with the "semicore" $4p^6$ density. A strict separation into core and valence states does not seem to be possible. As already shown in the case of similar problems related to the study[27–29] of II-VI semiconductors, inclusion of the nonlinear core correction[30] (NLCC) might possibly improve the results, but this is out of the scope of the present paper.

We have also tested pseudopotentials for Ca (Sr) with only $4s^2$ ($5s^2$) valence electrons. The results are poor. In this case, the deviation of the phonon frequencies from experiment at the Γ and more noticeably at the X point are up to roughly 30%. It is also remarkable that the ground-state properties are independent of the choice of the reference configuration.

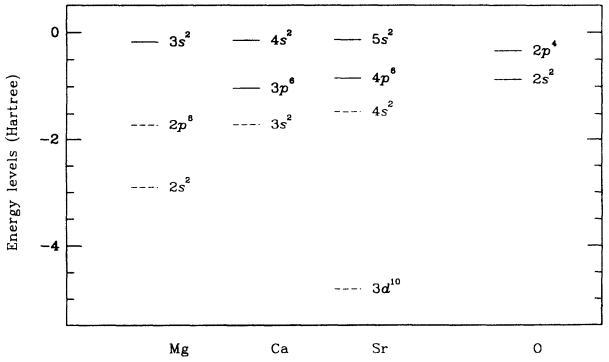

FIG. 1. The highest single-particle energy levels (in Hartree) for the elements Mg, Ca, Sr, and oxygen. The solid (dashed) lines indicate valence (core) atomic levels.

B. Equilibrium properties

The structural properties are determined by finding the minimum of the crystal total energy E as a function of the structural parameters. For the rocksalt structure the only relevant parameter is the lattice constant a. Using Murnaghan's equation of state[31] to determine the equilibrium lattice parameter one also obtains the bulk modulus B_0 and its derivative B_0' with respect to pressure as a by-product.

The converged results are shown in Table II and are compared with the corresponding experimental data. The deviation of the lattice constant from experiment is smaller than 2% in each case. The agreement of the bulk modulus with experiment is acceptable. Available

TABLE II. Equilibrium lattice parameter a (a.u.), bulk modulus B_0 (Mbar), pressure derivative of the bulk modulus B_0', Szigeti effective charges Z_S^*, given in terms of the Born effective charges as $Z_S^* = 3Z_B^*/(\epsilon_\infty + 2)$, and static (with clamped nuclei) dielectric constant ϵ_∞. The energy cutoffs for MgO, CaO, and SrO are 65, 55, and 60 Ry, respectively.

		a	B_0	B_0'	Z_S^*	ϵ_∞
MgO	theor.	7.87	1.62	4.2	1.15	3.14
	expt.	7.97[a]	1.64[b]		1.20[a]	2.94[a]
CaO	theor.	8.91	1.24	4.4	1.20	3.89
	expt.	9.09[a]	1.11[c]		1.18[a]	3.27[a]
SrO	theor.	9.64	0.98	4.0	1.26	3.94
	expt.	9.75[a]	0.91[c]		1.22[a]	3.47[a]

[a]Reference 4 and references therein.
[b]Reference 39.
[c]Reference 40.

TABLE III. Phonon frequencies (THz) calculated at the high-symmetry points Γ, X, and L, for the three compounds considered in this work. Experimental data are in parentheses.

	MgO[a]	CaO[b]	SrO[c]
Γ_{TO}	11.72 (12.23)	8.90 (9.05)	6.31 (6.72)
Γ_{LO}	21.25 (21.52)	17.08 (17.24)	14.28 (14.54)
X_{TA}	8.62 (8.96)	6.41 (6.48)	3.85 (3.87)
X_{LA}	12.59 (12.65)	9.62 (8.80)	6.04 (5.92)
X_{TO}	13.37 (13.29)	9.61 (9.40)	7.29 (7.50)
X_{LO}	16.55 (16.61)	11.74 (12.00)	9.20 (9.91)
L_{TA}	8.20 (8.64)	6.10 (5.85)	3.37 (3.33)
L_{LA}	16.40	11.64 (11.03)	7.11 (7.14)
L_{TO}	10.71 (11.05)	9.82	9.00 (8.35)
L_{LO}	17.07	14.58 (14.17)	13.47 (12.94)

[a]Experimental data from Refs. 41, 42.
[b]Experimental data from Refs. 43–46.
[c]Experimental data from Refs. 43, 47.

results from all electron calculations for MgO and CaO (Ref. 32) are very close to the results given here supporting the use of soft norm-conserving pseudopotentials.

The theoretical values for the static high-frequency dielectric constant, also reported in Table II, are overestimated, a fact which is typical for this kind of calculation and which has been related to the use of the LDA.[33,34]

C. Phonon dispersion curves

The results of the calculation for the phonon dispersion curves of MgO, CaO, and SrO along several symmetry directions and for the density of states (DOS) are shown in Figs. 2–4. Some numerical values at the high-symmetry points Γ, X, and L are also reported in Table III. The strongly attractive p potential of the oxygen is the dominating factor for the convergence behavior. The kinetic-energy cutoffs specified in Sec. II D guarantee converged values also for the dynamical properties.

The overall agreement with the available optical and neutron-scattering data for the three compounds is very good. Furthermore, frozen-phonon calculations[35] for MgO at the Γ and X points show similar agreement. This gives confidence in a high predictive power of the method for the experimentally unknown features of the phonon dispersion. The typical features, namely, the strong LO-TO splitting and the weakening of the LO-phonon mode along the ΓL direction, are well reproduced.

In the case of SrO the optical branches deviate from the neutron-scattering data, especially at the X and L points. The reason for the lesser degree of accuracy may possibly be related to the overlap of the filled $3d^{10}$ shell with the valence states of Sr as discussed in Sec. III A.

Additionally, the neutron-scattering data are taken at room temperature. The comparison with the low-temperature optical data shows a slightly better agreement of our calculations with experiment. This might be a hint at the presence of anharmonicities. However, we believe that the main differences are probably caused by neglecting the NLCC and not by the obviously small effects of anharmonicities; cf. Fig. 4.

Finally, in Table IV we present the sound velocities di-

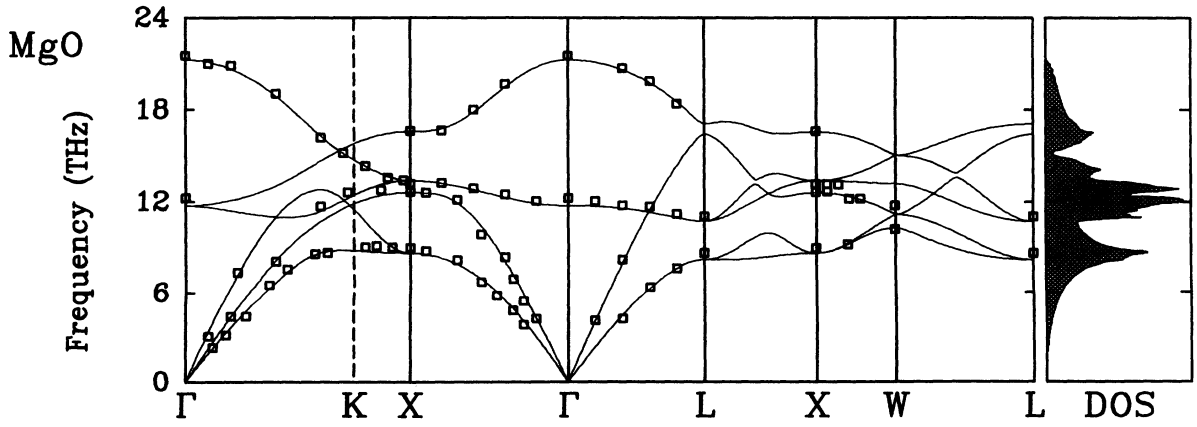

FIG. 2. Calculated phonon dispersion curves and density of states (DOS) for MgO. Experimental neutron-scattering data are denoted by open squares (from Ref. 42).

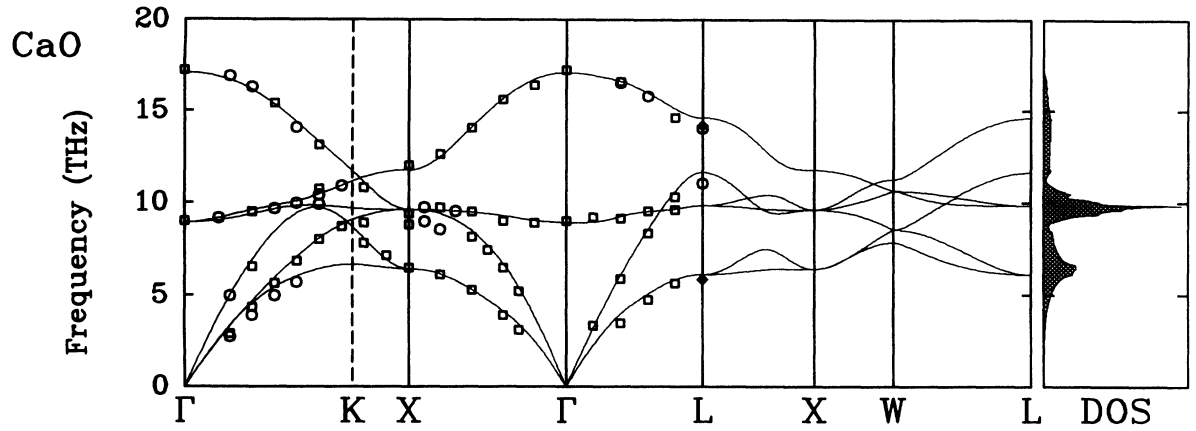

FIG. 3. Calculated phonon dispersion curves and density of states (DOS) for CaO. Experimental neutron-scattering data are denoted by open squares (from Ref. 44) and open circles (from Ref. 45). Optical data at L are indicated by solid diamonds (from Ref. 46).

rectly calculated from the slope of the acoustical branches in the long-wavelength limit. The experimental values were derived from the corresponding elastic constants. Typical deviations from experimental data are 5%, with somehow larger deviation for the sound velocities of the transversal branches of CaO.

D. Charge fluctuations

The principal shortcoming of empirical shell (or deformation-dipole) models, namely, their failure to fit the longitudinal-mode frequencies along the [111] direction in the alkali halides and alkaline-earth oxides, has led to the introduction of a breathing degree of freedom,[36] i.e., of a monopolelike charge fluctuation of the electronic shell. The breathing-shell model can be mapped onto a model[38] in which charge is transferred from one ion to another during a lattice vibration.

In order to test these physically different models we have investigated the phonon-induced charge changes for MgO and CaO, in particular at the L point, where one finds the strongest effects, and at the X point, where the effect is absent.

For the X point we have found only dipole excitations and no breathinglike behavior, in agreement with classical models. Thus, we will concentrate in the following on the L point.

Along the [111] direction the rocksalt structure has the fcc close-packed stacking order $ABA'B'A''B''AB\ldots$ with alternating planes, each of them containing only one type of ion. The eigensolutions of the dynamical matrix at the L point (and at the X point) can be separated into purely longitudinal or transverse modes.

In Figs. 5–10 we show the change $\Delta\rho_{\mathbf{q}}^{j}(\mathbf{r})$ of the charge density, Eq. (6), associated with various phonon modes j at the L point in the form of contour plots. In all these figures, dotted (solid) lines correspond to charge

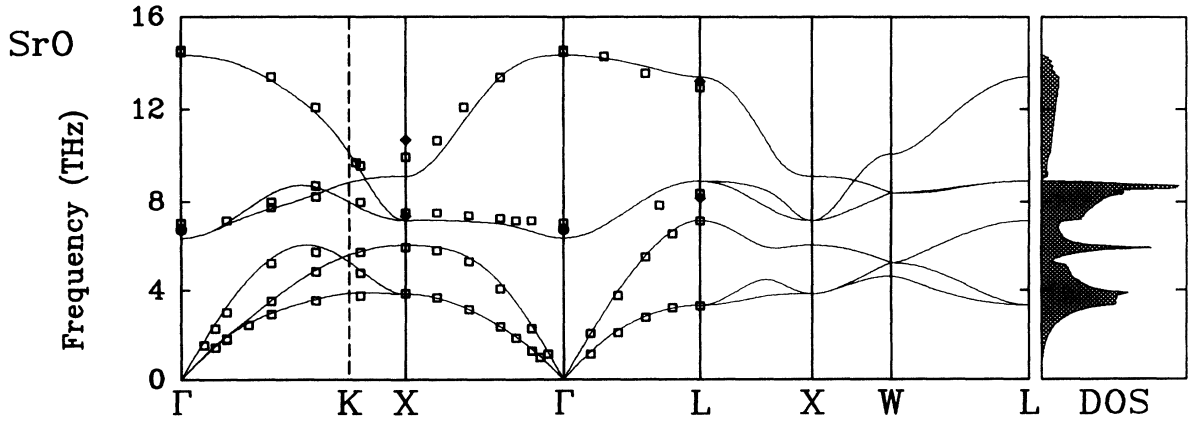

FIG. 4. Calculated phonon dispersion curves and density of states (DOS) for SrO. Experimental neutron-scattering data are denoted by open squares (from Ref. 47). Optical data for some modes at X and L point are indicated by solid diamonds (from Ref. 46), whereas low-temperature optical data at Γ are denoted by solid circles (from Ref. 43).

TABLE IV. Sound velocities (10^5 cm/s) along several high-symmetry directions. The subscripts L und T denote longitudinal and transverse branches, respectively. The experimental values have been derived from the experimental elastic constants.

		v_L [100]	v_T	v_L [110]	v_{T_1}	v_L [111]	v_T
MgO	theor.	9.22	6.47	9.81	5.52	10.01	5.85
	expt.[a]	8.99	6.58	9.80	5.30	10.06	5.76
CaO	theor.	8.88	5.77	8.76	5.95	8.73	5.89
	expt.[a]	8.23	4.93	8.21	4.96	8.21	4.95
SrO	theor.	6.47	3.72	6.31	3.96	6.23	3.89
	expt.[b]	6.21	3.49	6.03	3.78	5.98	3.69

[a]Reference 4 and references therein.
[b]Reference 37.

accumulation (depletion). The separating zero-contour line is given by a heavy solid line. Note the different scales for the contour lines in the different figures.

In the longitudinal and transverse acoustic modes, nearest cation planes are vibrating with opposite phases relative to the oxygen planes which are at rest.

Figures 5–8 relate to longitudinal acoustic modes. Figures 5 and 6 show results for a plane normal to the **q** vector and containing the oxygen. The breathing of the oxygen anion is obvious: Charge fluctuates from the outer towards the inner region of the anions with the cations moving away. This effect is strongest for MgO.

Figures 7 and 8 show results for a plane that contains the wave vector. For MgO and CaO two completely different situations arise: Due to an ionization degree of

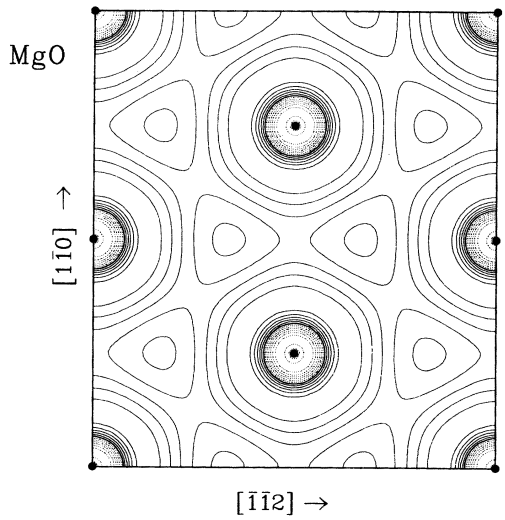

FIG. 5. Contour plot of the charge-density difference for MgO in the (111) plane for an LA phonon at the L point, $\mathbf{q} = (1,1,1)\pi/a$. The plane contains only oxygen ions. The oxygen sites are indicated by solid circles. Two subsequent contour lines are separated by 0.15 times a value of $0.11e/\text{Å}^3$ which corresponds to the absolute maximum of the charge-density difference. The cations in the plane above and below are moving away from this plane, resulting in a strong breathing effect for the oxygen ion.

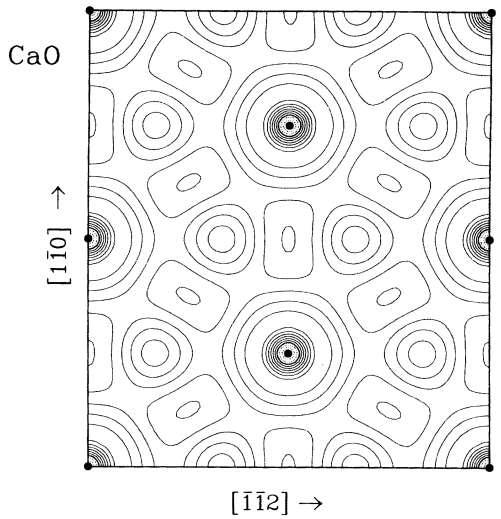

FIG. 6. Same as Fig. 5 but for CaO and for an absolute maximum of $0.08e/\text{Å}^3$.

roughly 2 of the Mg ion it is the bare ion core which is moving (cf. Table I). This is in contrast to Ca where the remaining six valence electrons can screen the electric field caused by the motion of the ions: A large dipole is induced at the site of the Ca ions; see Fig. 8. The development of the dipole moment is the main effect in CaO, and the electric screening results in a smaller charge deformation at the oxygen than in the case for MgO (Fig. 7). Note the very different scales of the contour plots; bringing Figs. 7 and 8 to the same scale leads to very similar pictures for the charge fluctuations around the oxygen ions (with only slightly smaller effects in the case

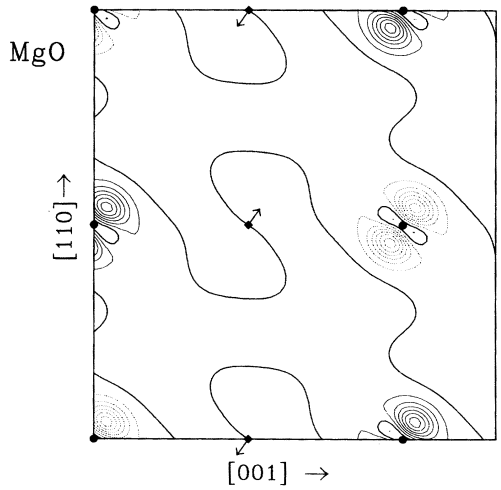

FIG. 7. Contour plot of the charge-density difference for MgO in the ($\bar{1}$10) plane. The ground-state density is perturbed by an LA phonon at the L point, $\mathbf{q} = (1,1,1)\pi/a$. Two subsequent contour lines are separated by 0.15 times a value of $0.72e/\text{Å}^3$ which corresponds to the absolute maximum of the charge-density difference. The oxygen sites are indicated by solid circles, the magnesium sites by solid diamonds. The displacements of the cations are along the arrows.

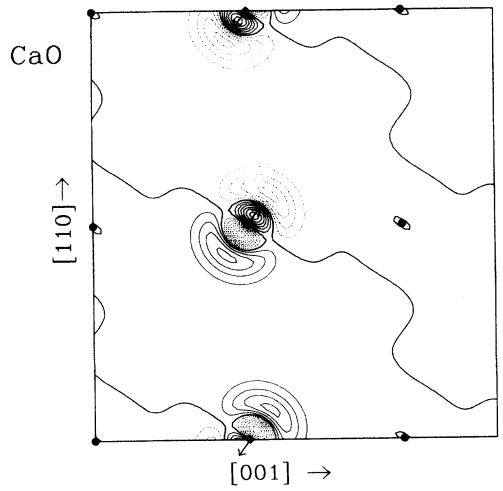

FIG. 8. Same as Fig. 7 but for CaO and with an absolute maximum of $6.88e/\text{Å}^3$.

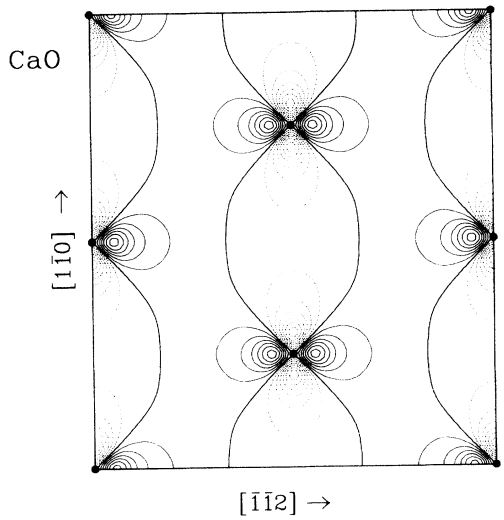

FIG. 10. Same as Fig. 9 but for CaO.

of CaO as mentioned) and, of course, leaves the zero-intensity contour lines unchanged. In contrast to the results shown in Figs. 5 and 6 the monopolelike charge fluctuation here is superimposed by a quadrupolar one.

We find a similarly significant response of the oxygen associated with the (degenerate) transverse acoustic modes. Figures 9 and 10 show this sensitivity of oxygen in form of quadrupole excitations, caused by motion of the cations in the parallel planes above and below the plotted one.

In the transverse and longitudinal optic modes the oxygen-ion planes are moving against the cation planes (at rest). For Ca we have found a similar response as for oxygen. The breathing of Ca in the LO mode is not as strong as that of oxygen, but it still exists. For Mg there is no polarizable charge, and the effects are carried over to oxygen.

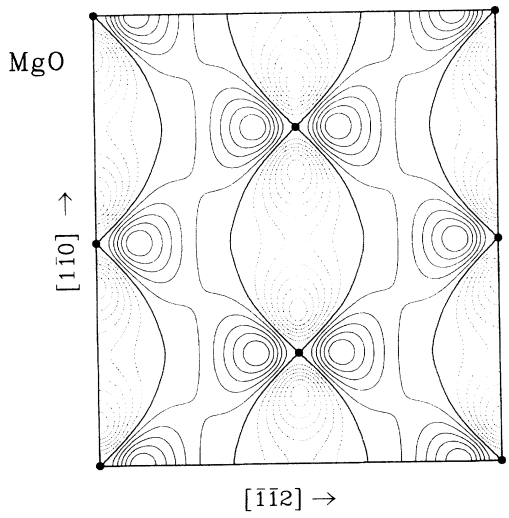

FIG. 9. Same as Fig. 5 but for a TA phonon and for an absolute maximum of $0.09e/\text{Å}^3$. The cations in the plane above and below are moving parallel to this plane along the [$\bar{1}\bar{1}$2] direction.

Thus, for longitudinal displacements there is a breathing effect at the oxygen ion in the plane perpendicular to the ion displacements and, to a lesser degree, at the Ca ion. This picture supports the breathing-shell model of Schröder.[36] However, while the breathing effect of the model is a short-range effect, leading to a decrease of the shell radius with approaching neighbors, it is actually an effect of the Coulomb interaction of the oxygen electrons with the positively charged neighbors, leading to an increase of the radius. The effect on the phonon frequencies is the same in either case. In addition, the breathing effect is superimposed by a quadrupolar effect in a plane containing the displacements. There is no indication of a charge transfer from one ion type to the other in contrast to the charge-transfer model of Wakabayashi.[38]

IV. CONCLUSION

We have investigated the three alkaline-earth oxides MgO, CaO, and SrO as prototype oxides. We have shown that for the construction of the norm-conserving pseudopotentials it is necessary to treat the $3p^6$ Ca ($4p^6$ Sr) "semicore" states as valence states. The results of our parameter-free calculations exhibit an overall close agreement with experiment and thus have a high predictive power for the experimentally unknown features of the phonon dispersion. The results for the phonon dispersion of SrO exhibit a slight deviation from experiment, especially at the Brillouin-zone boundaries (X and L points). This, we believe, is related to the neglect of the nonlinear core correction. In contrast to this, the ground-state properties for all three compounds are well reproduced and do *not* depend on the choice of the valence configuration.

Furthermore, we have discussed charge fluctuations for MgO and CaO caused by several phonon modes at the X and L points. As suggested by the breathing-shell

model, we have found breathinglike behavior of the large polarizable oxygen ion at the L point. An additional quadrupolar effect is present which is not contained in the model. The calcium cation, too, exhibits a certain "multipole" polarizability, similar to oxygen. In contrast to this, there are only dipolelike excitations at the X point.

To obtain deeper insight into the polarization mechanism of the oxygen ion we have recently started calculations for CaF_2, hereby substituting the oxygen in CaO by the most electronegative element fluorine. Preliminary results have been obtained also for KF which is isoelectronic with CaO.

ACKNOWLEDGMENTS

The authors wish to thank Stefano Baroni for his intensive help and the stimulating discussions at the beginnings of this work. We also want to thank the *Deutsche Forschungsgemeinschaft* who partially supported this work under Contract No. SCHR123/8.

[1] G. D. Mahan, Solid State Ion. **1**, 29 (1980).
[2] P. W. Fowler and P. A. Madden, J. Phys. Chem. **89**, 2581 (1985).
[3] P. W. Fowler, R. W. Mum, and P. Tole, Chem. Phys. Lett. **176**, 439 (1991).
[4] M. J. L. Sangster and A. M. Stoneham, Philos. Mag. B **43**, 597 (1981).
[5] M. E. Limes and A. M. Glass, *Principles and Applications of Ferroelectrics and Related Materials* (Clarendon, Oxford, 1977).
[6] J. Redinger and K. Schwarz, Z. Phys. B **40**, 269 (1981).
[7] A. Lorda, F. Illas, J. Rubio, and J. B. Torrance, Phys. Rev. B **47**, 6207 (1993).
[8] A. Zupan, I. Petek, M. Causa, and R. Dovesi, Phys. Rev. B **48**, 799 (1993).
[9] P. I. Sorantin and K. Schwarz, Inorg. Chem. **31**, 567 (1992).
[10] K. M. Glassford and J. R. Chelikowsky, Phys. Rev. B **46**, 1284 (1992).
[11] K. M. Glassford and J. R. Chelikowsky, Phys. Rev. B **47**, 1732 (1993).
[12] M. Catti, A. Pavese, R. Dovesi, and V. R. Saunders, Phys. Rev. B **47**, 9189 (1993).
[13] N. E. Zein, Fiz. Tverd. Tela **26**, 3028 (1984) [Sov. Phys. Solid State **26**, 1825 (1984)].
[14] S. Baroni, P. Giannozzi, and A. Testa, Phys. Rev. Lett. **58**, 1861 (1987).
[15] P. Giannozzi, S. de Gironcoli, P. Pavone, and S. Baroni, Phys. Rev. B **43**, 7231 (1991).
[16] P. Pavone, K. Karch, O. Schütt, W. Windl, D. Strauch, P. Giannozzi, and S. Baroni, Phys. Rev. B **48**, 3156 (1993).
[17] H. Wendel and R. M. Martin, Phys. Rev. B **19**, 5251 (1979).
[18] K. Kunc and R. M. Martin, Phys. Rev. Lett. **48**, 406 (1982).
[19] M. T. Yin and M. L. Cohen, Phys. Rev. B **26**, 3259 (1982).
[20] L. J. Sham, Phys. Rev. **188**, 1431 (1969).
[21] R. Pick, M. H. Cohen, and R. M. Martin, Phys. Rev. B **1**, 910 (1970).
[22] C. Falter, Phys. Rep. **164**, 1 (1988).
[23] N. Troullier and J. L. Martins, Phys. Rev. B **43**, 1993 (1991).
[24] H. Hellmann, *Einführung in die Quantenchemie* (Deuticke, Leipzig, 1937); R. P. Feynman, Phys. Rev. **56**, 340 (1939).
[25] J. Perdew and A. Zunger, Phys. Rev. B **23**, 5048 (1981).
[26] D. J. Chadi and M. L. Cohen, Phys. Rev. B **8**, 5747 (1973).
[27] G. E. Engel and R. J. Needs, Phys. Rev. B **41**, 7876 (1990).
[28] A. Qteish and R. J. Needs, Phys. Rev. B **43**, 4229 (1991).
[29] A. Dal Corso, S. Baroni, and R. Resta, Phys. Rev. B **47**, 3588 (1993).
[30] S. G. Louie, S. Froyen, and M. L. Cohen, Phys. Rev. **26**, 1738 (1982).
[31] F. D. Murnaghan, Proc. Natl. Acad. Sci. USA **50**, 697 (1944).
[32] M. J. Mehl, R. E. Cohen, and H. Krakauer, J. Geophys. Res. **93**, 8009 (1988).
[33] S. Baroni and R. Resta, Phys. Rev. B **33**, 7017 (1986).
[34] S. de Gironcoli, S. Baroni, and R. Resta, Phys. Rev. Lett. **62**, 2843 (1989).
[35] A. De Vita, M. J. Gillan, J. S. Lin, M. C. Payne, I. Štich, and L. J. Clarke, Phys. Rev. Lett. **68**, 3319 (1992).
[36] U. Schröder, Solid State Commun. **4**, 347 (1966).
[37] P. R. Son and R. A. Bartels, J. Phys. Chem. Solids **33**, 819 (1972).
[38] N. Wakabayashi, Solid State Commun. **23**, 737 (1977).
[39] D. H. Chung and G. Simmons, J. Geophys. Res. **74**, 2133 (1969).
[40] Z. P. Chang and E. K. Graham, J. Phys. Chem. Solids **38**, 1355 (1977).
[41] J. R. Jasperse, A. Kahan, J. N. Plendl, and S. S. Mitra, Phys. Rev. **146**, 526 (1966).
[42] M. J. L. Sangster, G. Peckham, and D. H. Saunderson, J. Phys. C **3**, 1026 (1970).
[43] M. Galtier, A. Montaner, and G. Vidal, J. Phys. Chem. Solids **33**, 2295 (1972).
[44] D. H. Saunderson and G. Peckham, J. Phys. C **4**, 2009 (1971).
[45] P. R. Vijayaraghavan, X. Marsongkohadi, and P. K. Iyengar, in *Proceedings of the Symposium on Neutron Inelastic Scattering,* Grenoble, France, 1972 (IAEA, Vienna, 1972), p. 95.
[46] K. H. Rieder, B. A. Weinstein, M. Cardona, and H. Bilz, Phys. Rev. B **8**, 4780 (1973). The second-order Raman data are obtained from a comparative analysis with the available neutron-scattering data. Related to contributions of the entire Brillouin zone, the derived frequencies have a relatively poor precision in comparison with the neutron data, though, for the sake of clarity, we omitted some "unreliable" values.
[47] K. H. Rieder, R. Migoni, and B. Renker, Phys. Rev. B **12**, 3374 (1975).

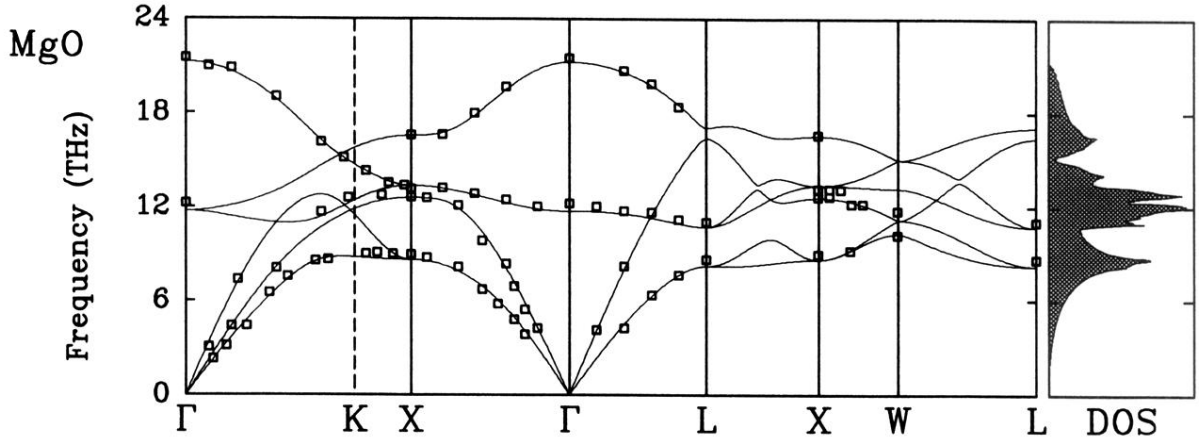

FIG. 2. Calculated phonon dispersion curves and density of states (DOS) for MgO. Experimental neutron-scattering data are denoted by open squares (from Ref. 42).

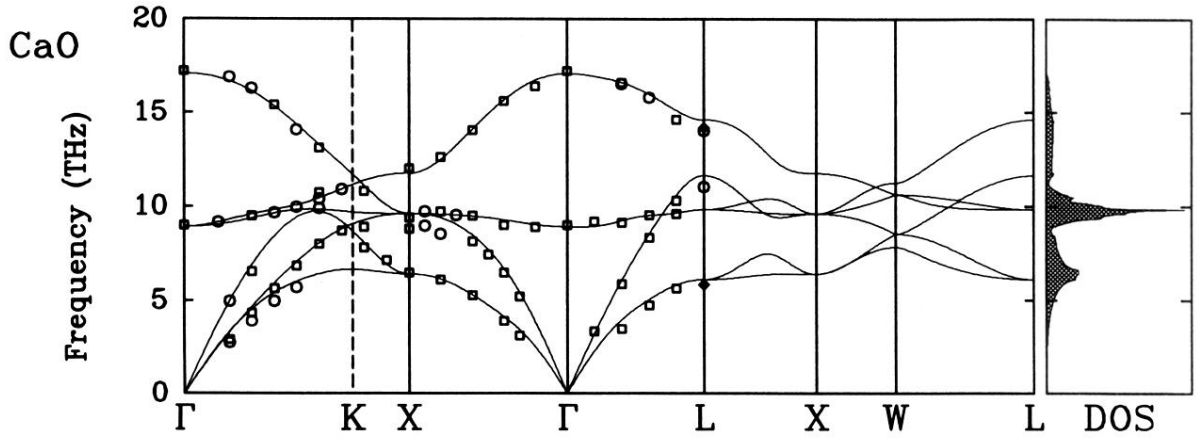

FIG. 3. Calculated phonon dispersion curves and density of states (DOS) for CaO. Experimental neutron-scattering data are denoted by open squares (from Ref. 44) and open circles (from Ref. 45). Optical data at L are indicated by solid diamonds (from Ref. 46).

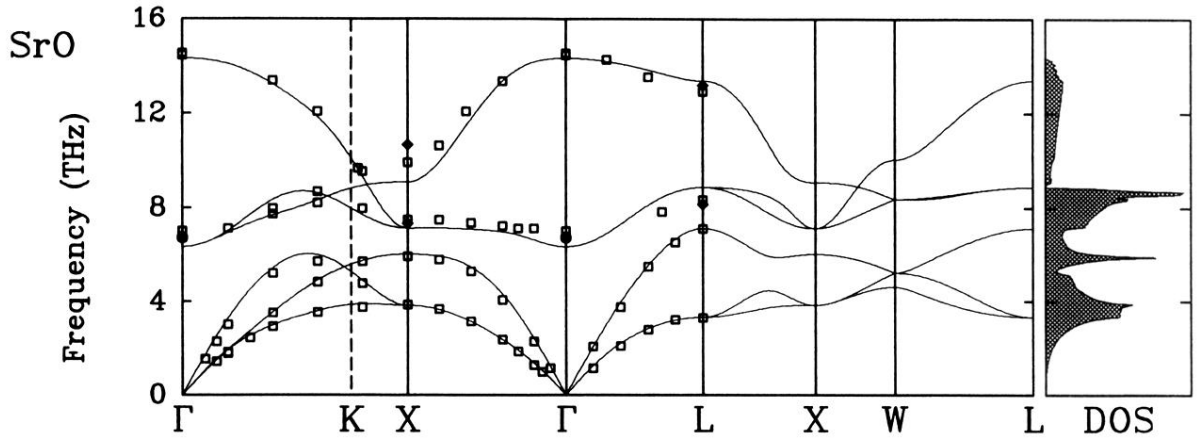

FIG. 4. Calculated phonon dispersion curves and density of states (DOS) for SrO. Experimental neutron-scattering data are denoted by open squares (from Ref. 47). Optical data for some modes at X and L point are indicated by solid diamonds (from Ref. 46), whereas low-temperature optical data at Γ are denoted by solid circles (from Ref. 43).